Seismic evidence that black-smoker heat flux is rate-limited by crustal permeability

Gillean M. Arnoux[1]*, Douglas R. Toomey[1], Emilie E. E. Hooft[1], William S. D. Wilcock[2], Joanna V. Morgan[3], Michael Warner[3], and Brandon P. VanderBeek[1]
[1]University of Oregon, Eugene, OR, [2]University of Washington Seattle Campus, Seattle, WA, United States, [3]Imperial College London, London, SW7, United Kingdom
*arnoux@uoregon.edu

Introduction

The heat flux of black-smoker hydrothermal systems is thought to be primarily controlled by localized magma supply and crustal permeability. Nevertheless, the structure of crustal permeability beneath such systems and its influence on hydrothermal heat flux remains unclear. Here we apply 3D full-waveform inversion[1] to seismic data from the hydrothermally active Endeavour segment of the Juan de Fuca Ridge to image the upper crust in high resolution. We conclude that black-smoker heat flux is rate-limited by an evolving, strongly heterogeneous permeability structure within the magmatic-hydrothermal reaction zone that results from an interplay between fracturing induced by localized magma chamber inflation and clogging of permeability by hydrothermal deposits.

ETOMO experiment

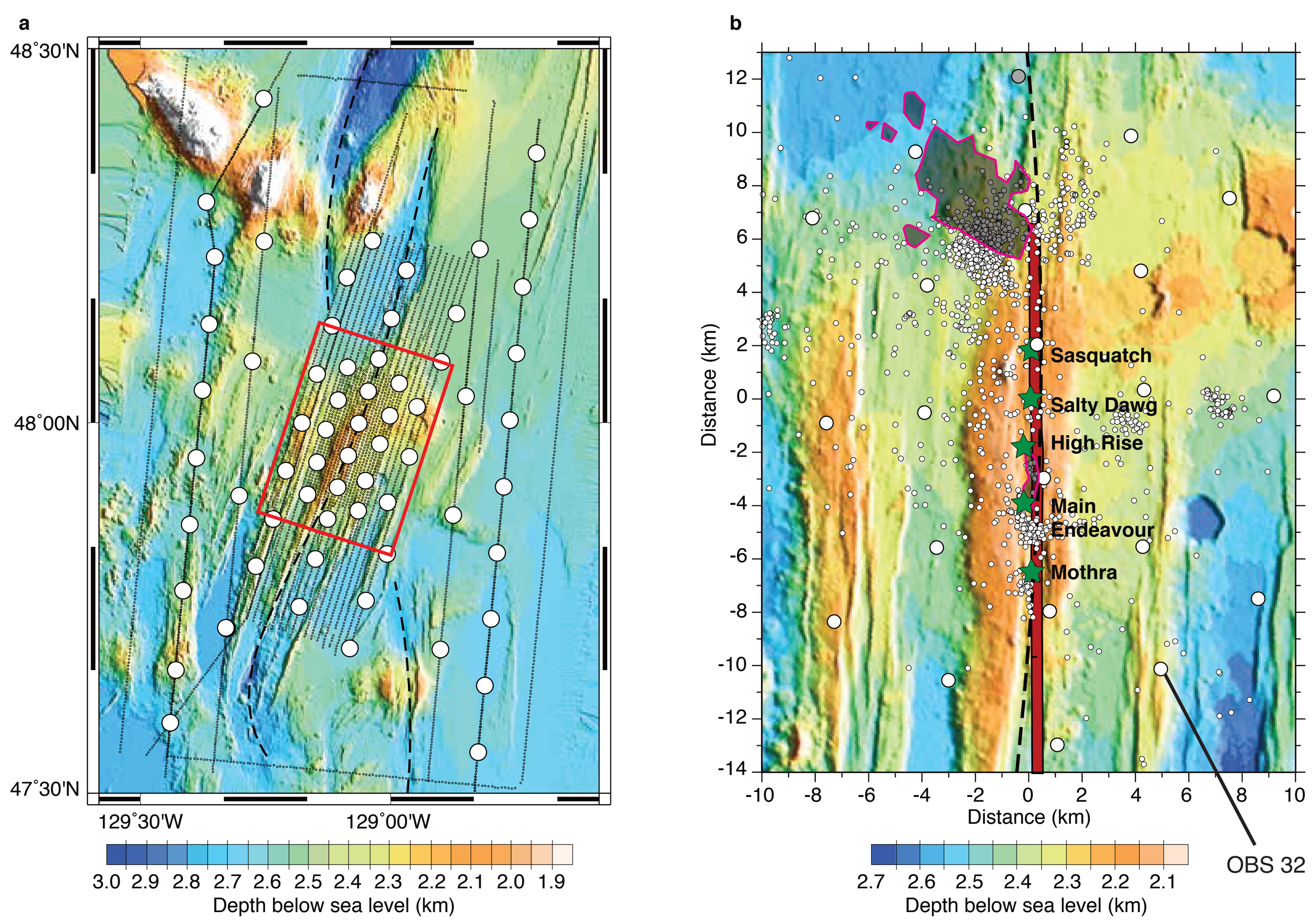

Figure 1 I (a) The Endeavour tomography (ETOMO) experiment configuration. (b) Crustal grid of the ETOMO experiment. Magenta contours shows areas with earthquake densities >20 events per km^2 recorded during the February 2005 swarm[4] and white dots are epicenters of post-swarm earthquakes that occurred between October 2005 and June 2006 (ref. 5). Dashed black line shows the plate boundary and green stars indicate hydrothermal vent fields.

- The Endeavour segment hosts five long-lived hydrothermal vents (green stars, Fig. 1b) that mine heat from an axial magma chamber (bold red line, Fig. 1b)[2,3].
- The crustal grid of the ETOMO experiment was designed to constrain the thermal and magmatic structure underlying the Endeavour hydrothermal system.

Full-waveform inversion

- FWI is applied to data from the dense crustal grid to develop high resolution models of the crust beneath well-studied hydrothermal vent fields.
- FWI uses an acoustic approximation to the wave equation and includes the kinematic effects of P-wave anisotropy; during the inversion, velocity is iteratively updated whereas anisotropy is held constant[1].
- A previous travel-time tomography study provides a three-dimensional starting model of upper crustal P-wave velocity and anisotropy[6].
- Data are windowed arround first-arriving crustal refractions owing to unconstrained velocity and anisotropy structure at mid- to lower-crustal depths in starting model.

Acknowledgements

The 3D FWI code used in this study was developed through industrial sponsorship managed by the Industry Technology Facilitator (ITF), UK. The experiment and analysis were supported by the NSF under grants numbered OCE-0454700 to the University of Washington and OCE-0454747 and OCE-0651123 to the University of Oregon.

References

1. Warner, M., Ratcliffe, A., Nangoo, T., Morgan, J., Umpleby, A., Shah, N., Vinje, V., Steki, I., Guasch, L., Win, C., Conroy, G., and Bertrand, A. (2013). Anisotropic 3D full-waveform inversion. Geophys ics, 78(2), R59-R80.
2. Van Ark, E. M., R. S. Detrick, J. P. Canales, S. M. Carbotte, A. J. Harding, G. M. Kent, M. R. Nedimovic, W. S. D. Wilcock, J. B. Diebold, and J. M. Babcock (2007). Seismic structure of the Endeav our Segment, Juan de Fuca Ridge: Correlations with seismicity and hydrothermal activity. Journal of Geophysical Research: Solid Earth (1978–2012), 112(B2).
3. Carbotte, S. M., J. P. Canales, M. R. Nedimovic, H. Carton, and J. C. Mutter (2012), Recent seismic studies at the East Pacific Rise 8°20– 10°10 N and Endeavour segment: Insights into mid-ocean ridge hydrothermal and magmatic processes, Oceanography, 25(1), 100–112.
4. Hooft, E. E., Patel, H., Wilcock, W., Becker, K., Butterfield, D., Davis, E., ... & Stakes, D. (2010). A seismic swarm and regional hydrothermal and hydrologic perturbations: The northernEndeavour segment, February 2005. Geochemistry, Geophysics, Geosystems, 11(12).
5. Weekly, R. T., Wilcock, W. S., Hooft, E. E., Toomey, D. R., McGill, P. R., & Stakes, D. S. (2013). Termination of a 6 year ridge-spreading event observed using a seafloor seismic network on the Endeavour Segment, Juan de Fuca Ridge. Geochemistry, Geophysics, Geosystems, 14(5), 1375-1398.
6. Weekly, R. T., Wilcock, W. S., Toomey, D. R., Hooft, E. E., and Kim, E (2014). Upper crustal seismic structure of the Endeavour segment, Juan de Fuca Ridge from traveltime tomography: Implications for oceanic crustal accretion. Geochemistry, Geophysics, Geosystems, 15(4), 1296-1315.
7. Kellogg, J. P. (2011), A hydrographic transient above the Salty Dawg hydrothermal field, Endeavour Segment, Juan de Fuca Ridge, PhD. Thesis, University of Washington, Seattle.
8. Wilcock, W. S. D., Hooft, E. E. E., Toomey, D. R., McGill, P. R., Barclay, A. H., Stakes, D. S., and Ramirez, T. M. (2009), The role of magma injection in localizing black smoker activity, Nature Geo-science., 2, 509-513.
9. Carlson, R. L. (2010) How crack porosity and shape control seismic velocities in the upper oceanic crust: Modeling downhole logs from Holes 504B and 1256D, Geochemistry, Geophysics, Geo-systems, 11, 1–15 (2010).

Results

i. Velocity structure

- **FWI improves the resolution of the travel-time tomography results by a factor of four.**
- **A low-velocity anomaly 2-3 km beneath the ridge axis (Fig. 3b) correlates with the location of the axial magma chamber (AMC) reflector[2,3].**
- **Along-axis velocity variations directly above the AMC reflector correspond with swarms of seismicity and the heat fluxes of the overlying vent fields[7] (Fig. 3b).**
- **A shallow (1-2 km depth) low-velocity anomaly underlies the ridge axis (Figs 4 and 5) and correlates with the location of earthquakes that occurred during a 6-year spreading event[4,5].**

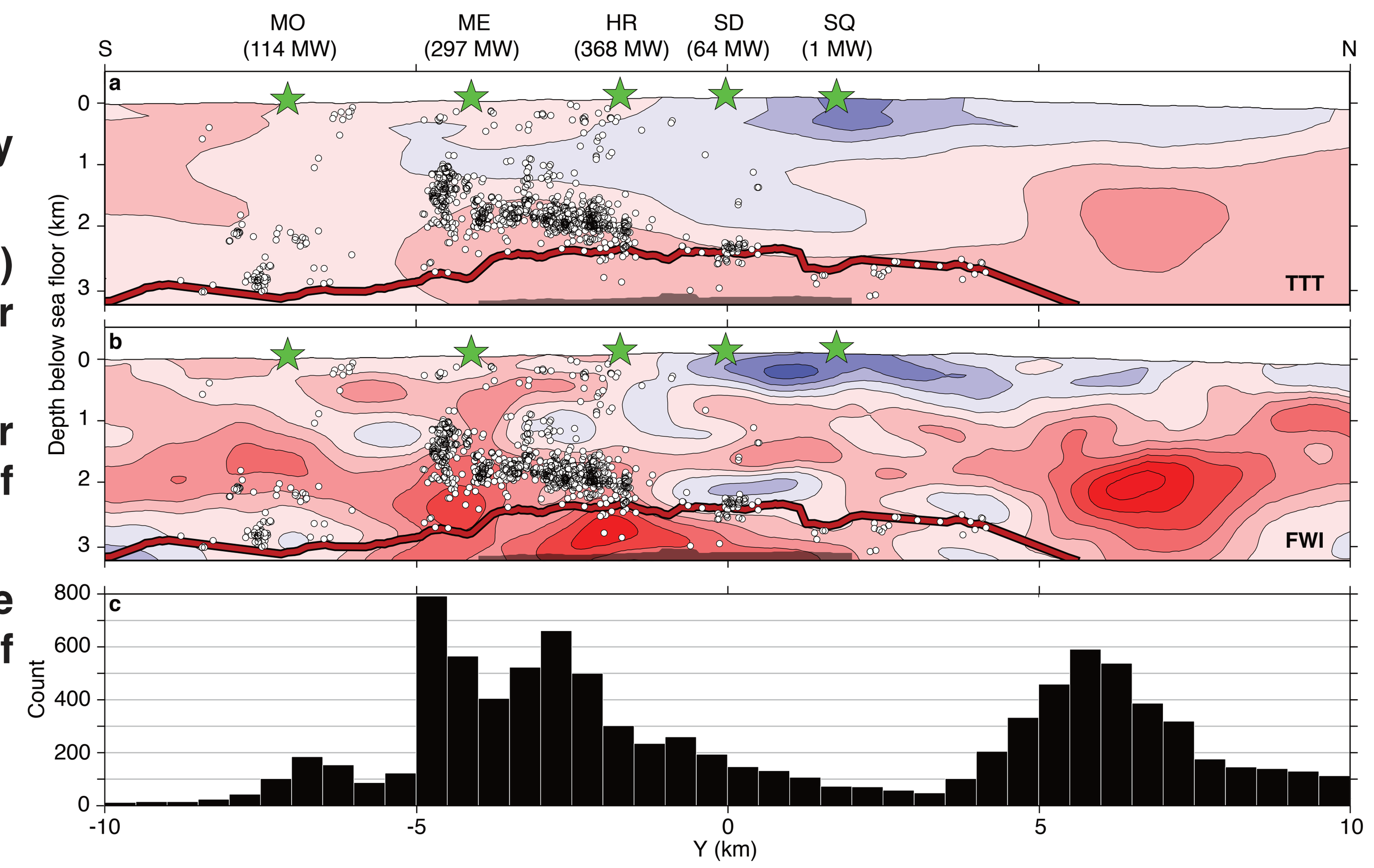

Figure 2 I Comparison between (a) travel-time tomography and (b) full-waveform inversion results. Sections show the locations of the vent fields (green stars), hypocenters for earthquakes recorded between 2003 and 2004 (white dots; ref. 8), and AMC reflector (bold red line). FWI model is masked in regions where the derivative weight sum is less than 10 (see resolution tests section). (c) Histogram of ~6000 earthquakes that occurred within 2 km of the ridge axis from 2003 to 2006.

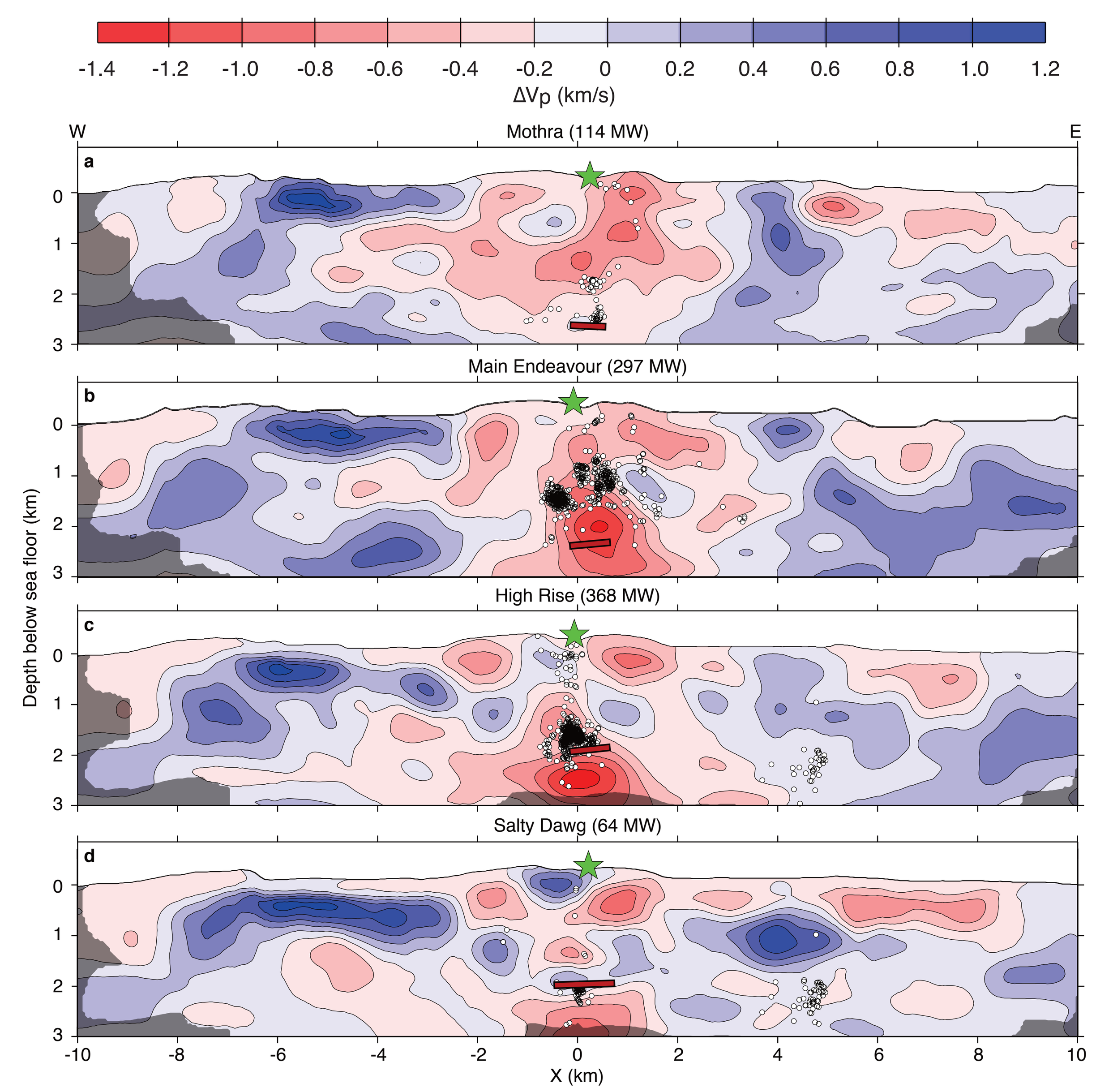

Figure 3 I Cross-axis sections showing FWI velocity anomalies beneath the vent fields, masked where the DWS is less than 10. Overlain are earthquakes recorded between 2003 and 2004 (white dots; ref. 8), vent field locations (green stars), and the AMC reflector[2] (bold red line). Heat fluxes are provided above each vent[8].

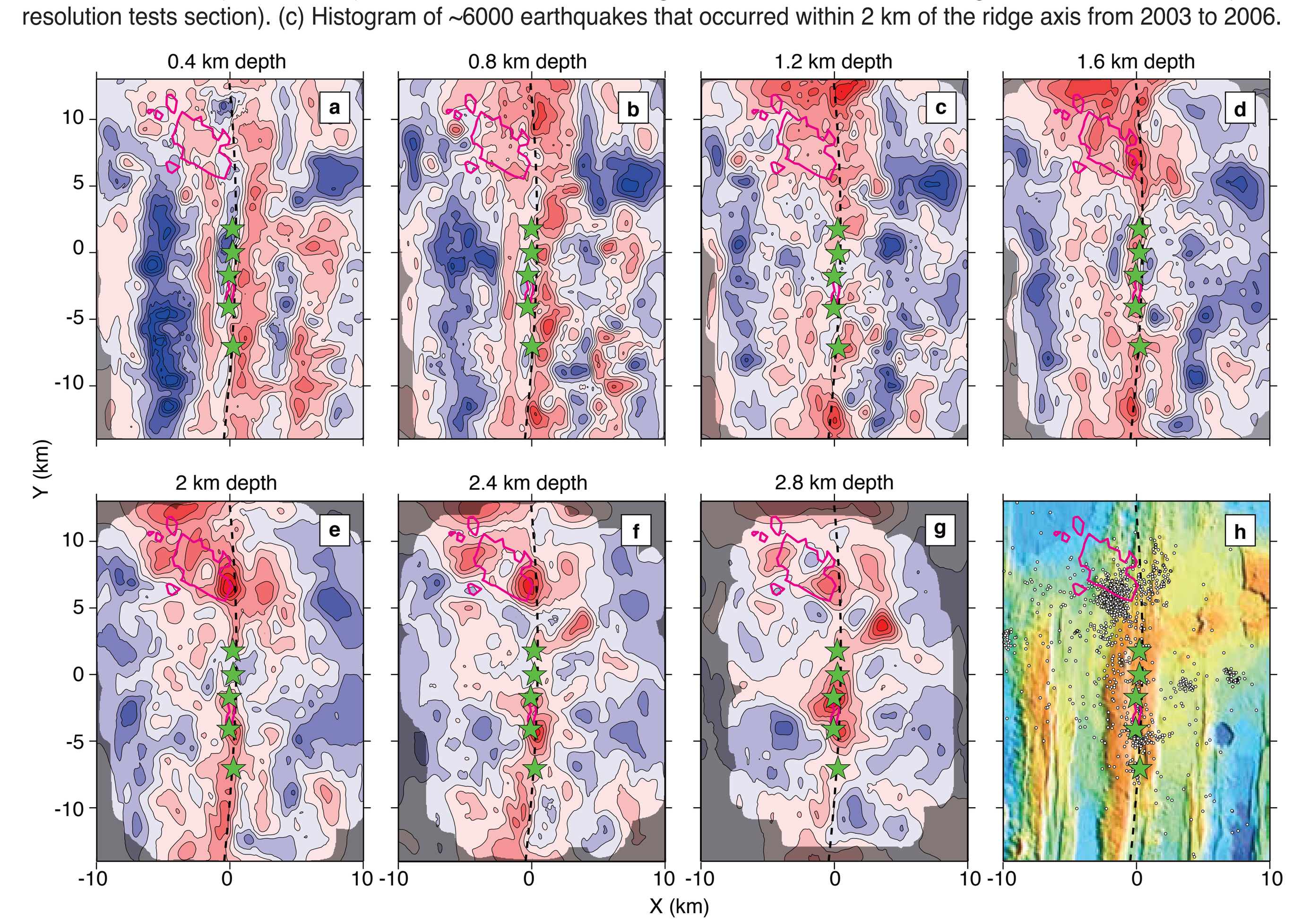

Figure 4 I Map view sections of three-dimensional segment-scale velocity anomalies. Plotted features are the same as those shown in Figure 1b. Sections are masked where the DWS is less than 10.

ii. Porosity and permeability structure

- **Large lateral velocity variations within the upper 1-3 km of crust are likely caused by localized changes in porosity, and by inference, permeability.**
- **The velocity structure is converted to porosity using empirically derived equations from borehole data of 6-15 Ma oceanic crust[9].**
- **Crustal porosity and permeability are strongly heterogeneous within the magmatic-hydrothermal reaction zone.**
- **Hydrothermal cementation, dike propagation, ridge-parallel faulting, and seismogenic cracking modify crustal permeability (Fig. 6).**

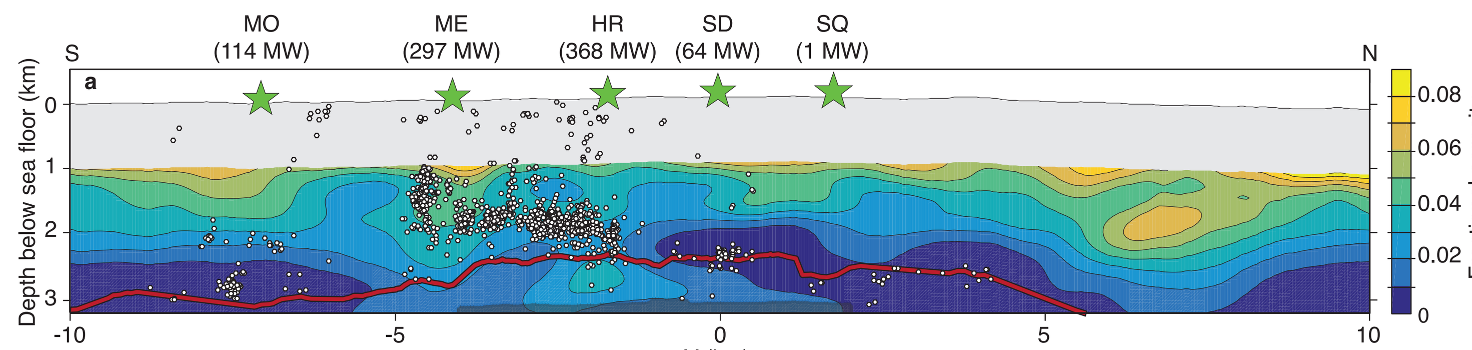

Figure 5 I Along-axis section of porosity structure for the model shown in Fig. 2a. Light grey regions indicates where values were omitted from calculations because of poor constraints on Layer 2A in very young oceanic crust.

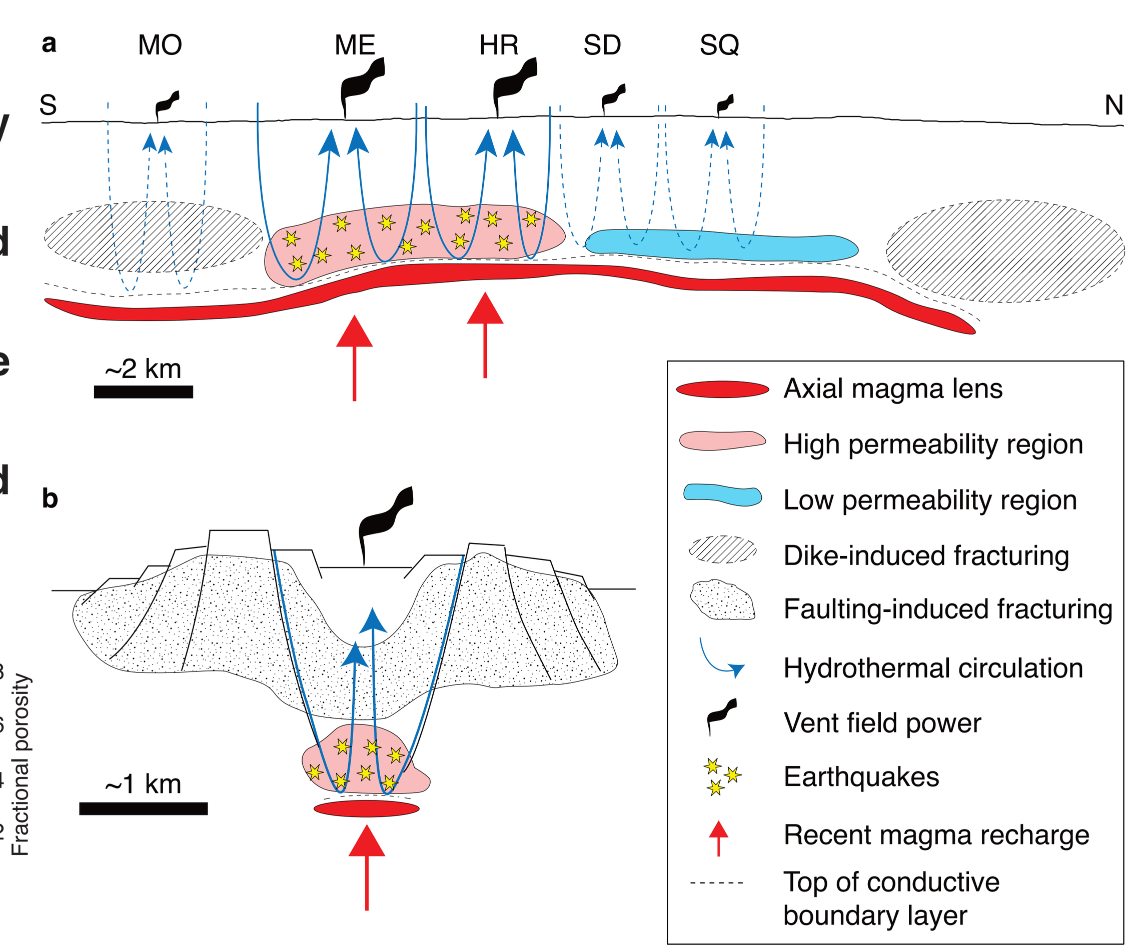

Figure 6 I Conceptual illustration for processes that modify crustal permeability (a) along-axis and (b) across-axis.

Conclusions

- **This study represents the first application of 3D FWI to an academic OBS dataset. We show that FWI is capable of improving the resolution of conventional travel-time tomography results by a factor of four when using a non-optimal dataset.**
- **We provide the first seismic constraints on the structure of the reaction zone that links the magmatic and hydrothermal systems and controls the patterns of heat transfer within a ridge segment.**
- **Velocity variations within the magmatic-hydrothermal reaction zone represent fluctuations in crustal permeability caused by seismogenic cracking induced by magma chamber inflation.**
- **Spatial and temporal variations in magma injection and induced seismogenic cracking generates an evolving, highly heterogeneous crustal permeability that governs the heat flux of black-smoker hydrothermal systems.**

Model fitness

- Phase residuals (Fig. 6a) between the field data and synthetics generated using the preferred FWI model are used to determine model fitness.
- Trace comparison of the observed and synthetic data (Fig. 6b) are also used.
- The preferred FWI model is capable of predicting the first 700 ms of data after the onset of the first arriving crustal refraction (black line, Fig. 6b) between offsets of 2.9-15 km. Data within 2.9 km and beyond 15 km offset are omitted because of wave interference and noise, respectively.

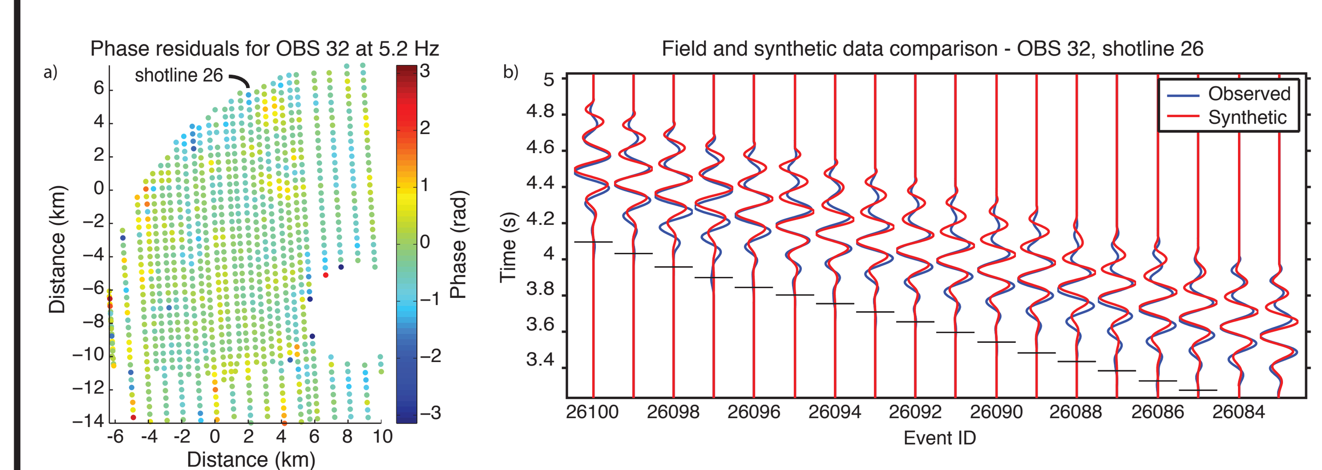

Figure 7 I (a) Phase residuals for shots recorded on OBS 32 (see Fig. 1b) within 2.9 to 15 km offset from the receiver and (b) trace comparison for a sequence of events from shotline 26.

Resolution tests

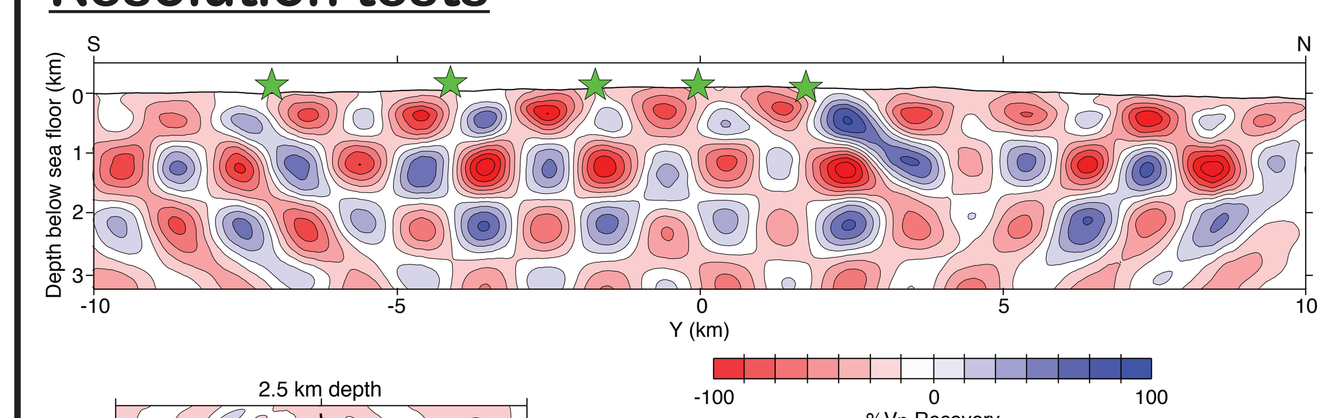

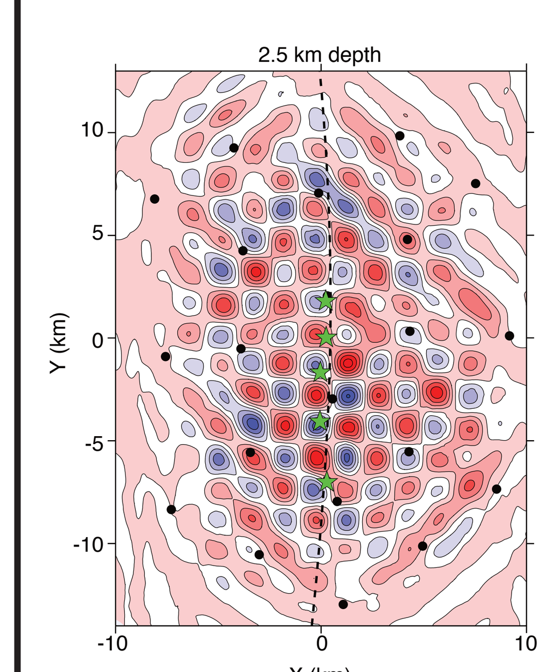

Figure 8 I Top: Recovered vertical checkerboard consisting of 1 km^3 columnar velocity perturbations of ±3% Vp applied to the starting velocity model. Left: Recovered horizontal checkerboard consisting of 1.5 km^3 velocity perturbations of ±3% Vp applied to the starting velocity model between 1.5-3 km depth. Overlain are vent fields (green stars), OBS locations (black dots), and the plate boundary (dashed black line).

- FWI is able to recover structures on the order of ~0.8-1 km^3, representing a fourfold improvement over the travel-time results.
- A derivative weight sum (DWS) - a spacial measure of the distribution of Pg raypaths in our model volume - threshold of 10 is used to masking (Figs 2-5).